PHOTONICS Research

Tunable non-Hermiticity through reservoir engineering

Xin Meng,[1] Zhiwei Hu,[1] Xingda Lu,[1] Wanxia Cao,[1] Xichang Zhang,[1] Haowei Li,[2] Ying Hu,[3,4] Wei Yi,[2,5] and Yanhong Xiao[3,4,*]

[1]Department of Physics, State Key Laboratory of Surface Physics and Key Laboratory of Micro and Nano Photonic Structures (Ministry of Education), Fudan University, Shanghai 200433, China
[2]CAS Key Laboratory of Quantum Information, University of Science and Technology of China, Hefei 230026, China
[3]State Key Laboratory of Quantum Optics and Quantum Optics Devices, Institute of Laser Spectroscopy, Shanxi University, Taiyuan 030006, China
[4]Collaborative Innovation Center of Extreme Optics, Shanxi University, Taiyuan 030006, China
[5]CAS Center For Excellence in Quantum Information and Quantum Physics, Hefei 230026, China
*Corresponding author: yxiao@sxu.edu.cn

Received 1 December 2021; revised 11 April 2022; accepted 4 May 2022; posted 4 May 2022 (Doc. ID 450166); published 15 August 2022

We experimentally demonstrate tunable non-Hermitian coupling in an atomic-vapor cell where atomic coherences in different optical channels are dissipatively coupled through atomic motion. Introducing a far-detuned light wall in the reservoir between the optical channels, we decorate the inter-channel coupling term so that it can be switched from dissipative to coherent. The tunable non-Hermiticity is then confirmed through measurements of the inter-channel light transport where the light-wall-induced phase shift is directly probed. Based on the tunable non-Hermiticity, we further discuss an exemplary scheme in which our setup can serve as a building block for the experimental study of exotic non-Hermitian criticality.

https://doi.org/10.1364/PRJ.450166

1. INTRODUCTION

Non-Hermitian Hamiltonians arise in quantum systems undergoing particle or information loss to their environment [1,2], and are responsible for rich and exotic non-Hermitian phenomena such as parity-time (PT) symmetry [3–10], non-Hermitian criticality [11–15], and non-Hermitian skin effects [16–24] and topology [16,25–29]. So far, non-Hermitian Hamiltonians have been experimentally implemented in quantum systems including single photons [30–32], atomic gases [33–40], semiconductor microcavities [41], nuclear spins in solids [42,43], trapped ions [44,45], and superconducting qubits [46]. In most of these experiments, non-Hermiticity is introduced through postselection under which quantum jump processes are irrelevant. The resulting conditional dynamics is driven by a non-Hermitian effective Hamiltonian, and is thus probability-non-conserving. By contrast, a unique experimental realization of non-Hermiticity exists in warm atomic-vapor cells where atomic coherences, also called spin waves [47], in spatially separated optical channels are dissipatively coupled according to the optical Bloch equations. Rather than direct particle or energy dissipation, the loss therein corresponds to the decaying atomic coherence under atomic thermal motion. In a prior series of experiments with atomic-vapor cells, (anti-)PT phases and phase transitions have been observed wherein the coexistence of the PT-related criticality and the quantum nature of the coherence coupling [48,49] offers intriguing prospects for applications in quantum control and device design. In these pioneering experiments, the coupling is nevertheless fixed to be dissipative, whereas it is desirable for practical purposes that the non-Hermiticity and the associated exotic features should be made tunable and on-demand.

In this work, we experimentally demonstrate, in a warm atomic-vapor cell, an easily switchable non-Hermitian coupling that can be either dissipative or coherent. As illustrated in Fig. 1, our setup consists of a pair of optically illuminated regions, or the optical channels, within an ensemble of warm atoms. The dissipative coupling between the spatially separated light fields is mediated by the atomic motion transporting and exchanging atomic coherence (that carries the information of light) within the two optical channels, and we identify atoms outside the illuminated regions as a non-Markovian reservoir. Introducing a far-detuned laser beam (denoted as the "light wall") into the reservoir, we achieve a tunable inter-channel coupling, such that the beam-splitter-type [50–52] interaction between the two channels can be captured by either a non-Hermitian or a Hermitian effective Hamiltonian, depending on the light-wall parameters. We confirm the tunability of the effective Hamiltonian by characterizing the light-wall-induced phase shift through the inter-channel light-transport measurements. We then discuss an experimentally accessible scheme in which the configuration implemented here can be used as a basic building block for more involved studies of

non-Hermitian criticality. Our experiment therefore not only offers a novel scheme for optical device design, but also provides a flexible tool for the quantum simulation of non-Hermitian physics.

2. RESULTS

For our experiment, we use a paraffin-wall-coated [53–55] ^{87}Rb vapor cell at a temperature of 40°C, housed within a four-layer magnetic shield to screen out the ambient magnetic field. As shown in Fig. 1, external lasers create two spatially separated optical channels (labeled Ch1 and Ch2) with inter-channel distance ∼1 cm, where atoms in each channel undergo standard Λ-type electromagnetically induced transparency (EIT). Specifically, an external cavity diode laser provides the light for the probe and control fields with orthogonal circular polarizations that couple the ground-state Zeeman levels $|F=2,m_F=0\rangle$ (labeled as $|1\rangle$) and $|F=2,m_F=2\rangle$ (labeled as $|2\rangle$) to an excited state $|F'=1,m_{F'}=1\rangle$ (labeled as $|3\rangle$) of the D_1 line. The control and probe beams have a diameter of about 1.5 mm, with input power of 80 μW and 8 μW, respectively. Between the two channels, a circularly polarized far-off-resonance red-detuned laser beam is shone through the vapor cell, with an elliptical cross section, about 2.5 cm in length (same as the diameter of the vapor cell) and 7 mm in width. We note that, since the control laser here is relatively weak, we have EIT instead of Autler–Townes splitting (ATS), which is a phenomenon occurring at a much higher laser power [56–60]. As shown in Section 4, the measured linewidth has a linear dependence on the laser power, and is below 100 Hz. Since the linewidth is much less than the excited-state linewidth (∼500 MHz Doppler broadened), our measurement is consistent with that of the EIT.

To measure the EIT spectra of a given channel, we record the probe field output intensity while sweeping a homogeneous

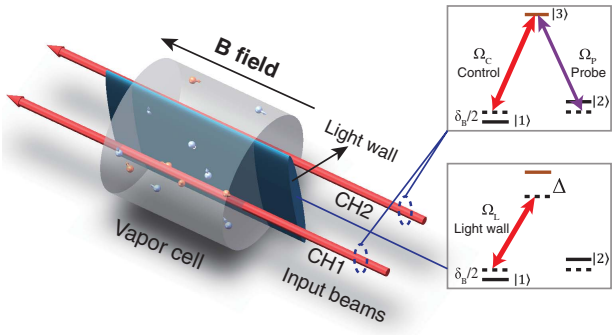

Fig. 1. Schematics of the tunable non-Hermiticity through reservoir engineering. Each of the two spatially separated optical channels within the atomic-vapor cell, Ch1 and Ch2, contains collinearly propagating weak probe and strong control fields (with Rabi frequency of Ω_p and Ω_c, respectively) operating under the condition of EIT. For the so-called "light wall," we introduce a light beam in between the two channels, which is far-detuned with respect to the center of the D_2 line transition of ^{87}Rb ($5S_{1/2}, F=1$ to $5P_{3/2}, F'=0,1,2,3$), with a narrow elliptical profile, and the same helicity as the control field. The inter-channel coherence transport is mediated by the atomic motion. Atoms traversing the light wall gain an average phase shift of θ_0 in ground-state coherence.

magnetic field generated by a solenoid inside the magnetic shield. By contrast, when comparing the probe output of both channels as we sweep the probe's phase in one of the channels, the magnetic field is switched off.

Under the optical Bloch equations, atomic coherences between the Zeeman states $|1\rangle$ and $|2\rangle$ in the two optical channels are dissipatively coupled with each other, as atoms traverse the reservoir under thermal motion. As a key element of our experiment, we introduce a far-detuned light wall in the reservoir, which shifts the hyperfine energy levels in a state-selective fashion, and imprints an extra phase onto the coherence as atoms pass through.

Specifically, the equations of motion for the atomic coherences satisfy

$$\begin{cases} \dot{\rho}_{12}^{(1)} = -\gamma_{12}'\rho_{12}^{(1)} + \Gamma_c\rho_{12}^{(2)} - \dfrac{\Omega_c^{(1)*}\Omega_p^{(1)}}{\gamma_{23}}, \\ \dot{\rho}_{12}^{(2)} = -\gamma_{12}'\rho_{12}^{(2)} + \Gamma_c\rho_{12}^{(1)} - \dfrac{\Omega_c^{(2)*}\Omega_p^{(2)}}{\gamma_{23}}, \end{cases} \tag{1}$$

where $\rho_{12}^{(i)}$ $(i=1,2)$ is the ground-state coherence of the ith channel, whose total effective decay rate is $\gamma_{12}' = \gamma_{12} + \Gamma_c + \Gamma_p^{(1)} + \Gamma_p^{(2)}$, where $\Gamma_p^{(i)} = \frac{|\Omega_c^{(i)}|^2}{\gamma_{23}}$ is the optical pumping rate, with γ_{12} and γ_{23} the decay rate of the coherence between states $|1\rangle$, $|2\rangle$ and $|2\rangle$, $|3\rangle$, respectively. Ω_c and Ω_p are the Rabi frequencies of the control and probe fields, respectively. Importantly, in the presence of the light wall, the inter-channel coupling rate Γ_c is dressed by an extra phase θ_0, and replaced by $\Gamma_c e^{i\theta_0}$.

The dissipative inter-channel coupling above gives rise to a beam-splitter-type interaction [61] effectively described by the Hamiltonian

$$\hat{H} = \hbar(g\hat{a}_1^\dagger\hat{a}_2 - g^*\hat{a}_2^\dagger\hat{a}_1)e^{i\theta_0}, \tag{2}$$

where $\hat{a}_1$ ($\hat{a}_2$) is the annihilation operator for the probe field in Ch1 (Ch2), and g is a complex coupling coefficient, with its phase given by $\phi_c^{(1)} - \phi_c^{(2)}$, where $\phi_c^{(1,2)}$ are the phases of the control fields in the corresponding optical channel. While $\theta_0 = 0$ in the absence of the light wall, its value is easily tunable by adjusting the intensity or detuning of the laser generating the light wall. Notably, when $\theta_0 = \pi/2$, the Hamiltonian [Eq. (2)] becomes Hermitian.

To experimentally confirm the analysis above, we first characterize the property of the light wall. In a paraffin-coated cell, the far-detuned beam of the light wall gives rise to a non-local, state-selective energy shift. This is because atoms can fly through the laser beams many times by bouncing off the vapor-cell wall, their ground-state coherence nearly intact. The light wall is therefore equivalent to an inhomogeneous global magnetic field that shifts and inevitably broadens the EIT spectrum. The impact of the light wall on the EIT spectrum is shown in Fig. 2, where the experimentally observed EIT spectra in Fig. 2(a) agree well with those from Monte-Carlo numerical simulations [40] in Fig. 2(b). Further, the observed spectral shift is proportional to the laser power [see Fig. 2(c)], while inversely proportional to its detuning [see Fig. 2(d)]. These observations derive from the phase imposed by the light wall, and form the basis for our control scheme below.

The effective Hamiltonian [Eq. (2)] governs the coupling-related evolution of the atomic coherences (or, equivalently, the

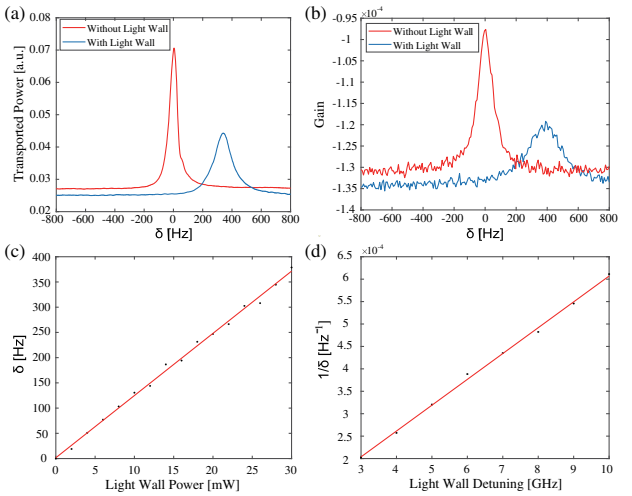

Fig. 2. Characterization of the light wall. Illustration of typical EIT spectra with (blue) and without (red) the light wall, obtained from (a) experiment and (b) Monte-Carlo simulations. (c) Measured EIT center shift versus laser power, with red detuning of 6 GHz. (d) Measured EIT center shift versus laser detuning, with laser power of 24 mW.

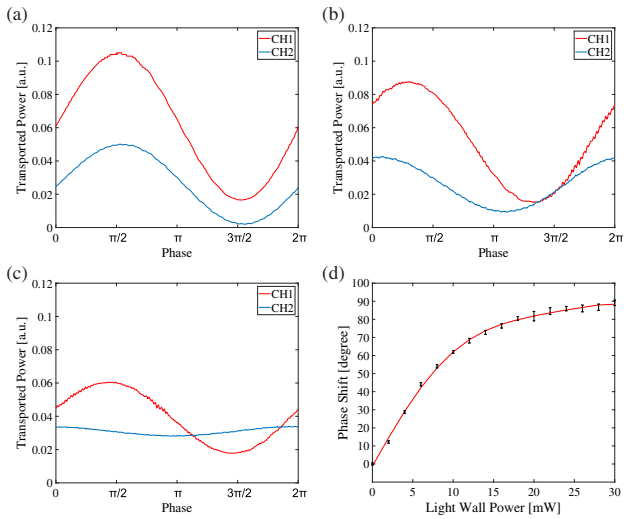

Fig. 3. Measurement of the light-wall-induced phase shift in the atomic spin wave. Light power output from the interference between the control and probe fields in Ch1 and Ch2, respectively, with (a) light wall turned off, (b) light-wall power of 6 mW, and (c) light-wall power of 30 mW. The inferred phase shifts of the spin wave are 0, $\pi/4$, and $\pi/2$ respectively. (d) Light-wall-induced spin wave phase shift versus light-wall power. The light-wall laser is red-detuned by 6 GHz.

probe fields) as the light traverses the vapor cell. Its impact therefore can be probed through the light transport where the light-wall-induced phase shift θ_0 manifests itself in the resulting intra- and inter-channel interference. To probe this phase shift, we first turn off the weak probe in Ch2 and slowly sweep the phase of the probe field in Ch1. In this case, the measured output probe field in Ch2 directly corresponds to the light transported from Ch1, thus containing information of the light-wall-induced phase shift.

We interfere a small fraction of the control fields with the probes using a half-wave plate in the output of each channel. The light-wall-induced phase is manifested in the phase shift between the measured output intensities of the two channels [Figs. 3(a)–3(c)], where $I_1 \propto \cos\theta_1$ and $I_2 \propto \cos(\theta_0 + \theta_1)$, consistent with theoretical predictions based on the Hamiltonian [Eq. (2)] [49]. Here $\theta_1 = \phi_p^{(1)} - \phi_c^{(1)}$ and $\phi_p^{(1,2)}$ are the phases of the input probe fields of the corresponding channels. When the laser power of the light wall increases, the phase shift should also increase, which is observed in Fig. 3. For a sufficiently large laser power of 30 mW, the phase shift can reach $\pi/2$, when the beam-splitter-type interaction becomes Hermitian. We note that the light-wall-induced phase θ_0 exhibits saturation behavior with increasing laser power, while the light-wall-induced EIT spectral shift is linear in laser power. This is because the phase shift θ_0 is approximately the product of the spectral shift and the effective interaction time between the atoms and the light wall. The interaction time is roughly the coherence lifetime and is inversely proportional to the EIT linewidth, which is broadened by the light-wall-induced effective magnetic field, as shown in Figs. 2(a) and 2(b). We have confirmed this analysis by reproducing the saturation behavior using Monte-Carlo simulations.

To further confirm the impact of the light wall, we study the output probe intensities without interfering it with the control fields, while both probe fields in Ch1 and Ch2 are switched on. As the phase of the input probe in Ch1 is slowly swept, we record the output probe fields' intensities in Ch1 and Ch2 separately, which, according to our theoretical derivations, should be $I_1 \propto \cos(\theta_1 - \theta_2 - \theta_0)$ and $I_2 \propto \cos(\theta_2 - \theta_1 - \theta_0)$, respectively. Here $\theta_2 = \phi_p^{(2)} - \phi_c^{(2)}$ and $\phi_{p,c}^{(2)}$ are the corresponding phases of the probe and control fields in Ch2. Apparently, the unsynchronized intensity output of the two channels originates from the phase interference of two processes: one is the reading and writing of the ground-state coherence by the control and the probe fields, featuring direction-dependent phases $\theta_1 - \theta_2$ and $\theta_2 - \theta_1$, respectively, and the other the direction-independent phase θ_0 from the light wall. This scheme is closely related to a recent proposal on nonreciprocity [62]. As shown in Fig. 4, the experimental observations agree well with theoretical predictions. In the absence of the light wall [see Fig. 4(a)], the two output probes change in a synchronized way; with the addition of the light wall [see Fig. 4(b)], the output intensities of the probes display a phase lag. It is worth noting that, compared to the case in Fig. 3, now the phase lag is $2\theta_0$. Under a higher laser power, the phase lag approaches π, demonstrating a fully out-of-phase behavior as shown in Fig. 4(c), which recovers the property of a conventional beam splitter (BS) commonly used in optical interferometry experiments. However, the remaining difference from the conventional Hermitian BS is that the light-wall-induced "Hermitian" BS here suffers additional loss, and is a manifestation of the Kramers–Kronig relation. Namely, the change in the probe field's phase (due to the ground-state coherence's phase change by the light wall) is associated with the additional absorption in the probe field.

The configuration demonstrated here serves as a flexible building block in implementing more complicated non-Hermitian models for the study of exotic non-Hermitian

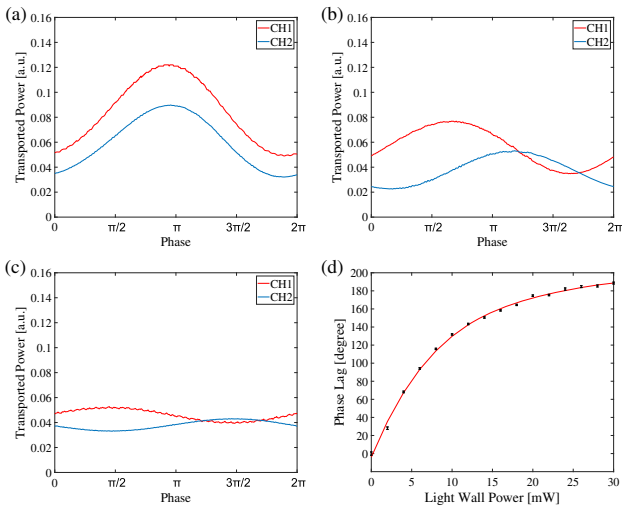

Fig. 4. Beam splitter with tunable non-Hermiticity. Transmitted probe powers in Ch1 and Ch2, with input probes in both channels turned on, with (a) absence of the light wall, (b) light-wall power of 6 mW, and (c) light-wall power of 24 mW, displaying a phase lag between the two channels of about $\pi/2$ and π for (b) and (c), respectively. (d) Light-wall-induced phase lag versus light-wall power.

criticality or topology. As a concrete example, we propose a minimal setup that involves three optical channels A, B, and C, and is readily accessible in an experiment using vacuum vapor cells without wall-coating. In such cells, adjacent optical channels couple through ballistic diffusion such that the next-nearest-neighbor coupling can be neglected [63]. As illustrated in Fig. 5(a), we assume that, between channels A and B, the phase factor in the coupling term g_0 is 1, and the light-wall-induced coherence' phase shift is θ_0; between channels B and C, the phase factor in the coupling term g_1 is $-i$, and the light-wall-induced phase shift is $\theta_1 = \pi/2$. Then, the effective non-Hermitian Hamiltonian is

$$\hat{H} = \delta\hat{a}^\dagger\hat{a} + g_0 e^{i\theta_0}\hat{b}^\dagger\hat{a} - g_0 e^{i\theta_0}\hat{a}^\dagger\hat{b} + g_1\hat{c}^\dagger\hat{b} + g_1\hat{b}^\dagger\hat{c}, \quad (3)$$

where $\hat{a}$, $\hat{b}$, and $\hat{c}$ are the annihilation operators for the probe beams in channels A, B, and C, respectively; the coupling terms g_0 and g_1 can be tuned by the distance between the channels as well as the laser beam size, and the on-site energy shift δ can be created through AC-Stark shift generated by an off-resonance laser beam within channel A [48]. As shown in Fig. 5, the non-Hermitian Hamiltonian [Eq. (3)] features highly tunable exceptional points, and offers an accessible minimal configuration where intriguing non-Hermitian phenomena such as higher-order exceptional point and exceptional-point encircling can be systematically probed using atomic-vapor cells. Specifically, the Hamiltonian has PT symmetry for $\theta_0 = 0$ and $\delta = 0$, whereas exceptional points are tunable through δ [see Fig. 5(c)]. The PT symmetry is broken when θ_0 deviates from 0 or $\delta \neq 0$ [see Figs. 5(d)–5(f)], offering a sensitive control for the study of non-Hermitian criticality at the exceptional points.

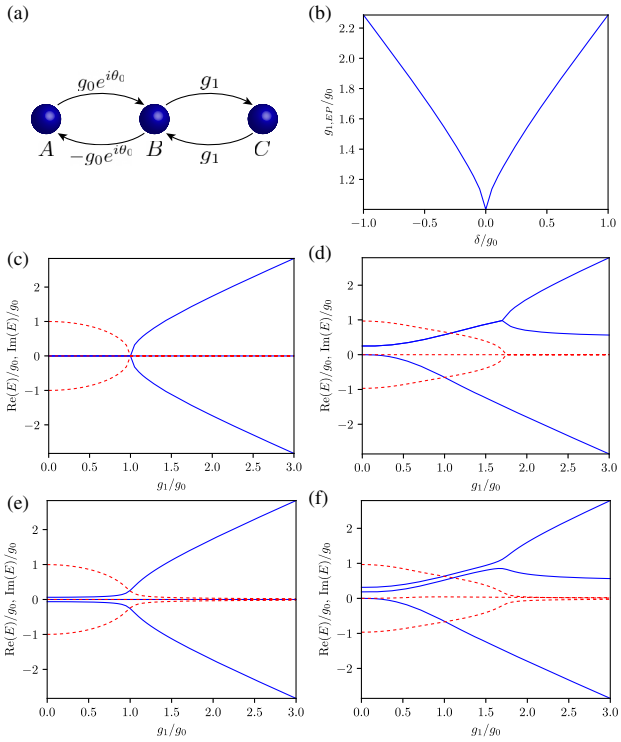

Fig. 5. (a) Schematic illustration of the proposed three-channel model in Eq. (3). (b) Location of the exceptional point as a function of δ for $\theta_0 = 0$. A third-order exceptional point only exists at $\delta = 0$. (c) Real (blue solid) and imaginary (red dashed) components of the eigenspectrum of Eq. (3), with $\delta = 0$ and $\theta_0 = 0$. A third-order exceptional point exists at $g_1/g_0 = 1$. (d) Eigenspectrum with $\delta/g_0 = 0.5$ and $\theta_0 = 0$; a second-order exceptional point remains at $g_1/g_0 = 1.73$. (e) Eigenspectrum with $\delta = 0$ and $\theta_0 = 0.02\pi$. (f) Eigenspectrum with $\delta/g_0 = 0.5$ and $\theta_0 = 0.02\pi$.

3. CONCLUSION

In conclusion, tunable non-Hermitian coupling between light modes is demonstrated in an atomic ensemble with the assistance of atomic motion and a light wall in the reservoir. The atomic spin wave picks up an extra phase when travelling through the light wall. The non-Hermiticity of the corresponding Hamiltonian is controlled by adjusting laser parameters of the light wall. While we confirm the tunability of the system through light-transport measurements, our setup can be applied as a building block for applications in quantum simulation of non-Hermitian physics and nonreciprocal devices [62,64–68]. Compared to existing studies of tuning non-Hermiticity in optical cavities and laser-array systems [69,70], our experiment is based on atom-optic coupling, which enables future quantum optical applications. In a recent experiment, the Hermiticity of a magnon–photon beam splitter in cold atoms was tuned by varying the laser detuning [61], while our method is suitable for spatial splitting of light and potential large-scale spatial multiplexing of quantum light sources [71].

4. METHODS

A. EIT Linewidth Measurement

In order to show that our experiment is in the regime of EIT, not ATS, we have measured the EIT linewidth as a function of

the laser power of the control field, in the range that covers our experimental condition. As shown in Fig. 6, the linewidth has a linear dependence on the laser power, and is less than 100 Hz, much narrower than the excited-state linewidth (~500 MHz Doppler broadened). These features are in contrast to those of ATS, whose linewidth is larger than the excited-state linewidth, and is proportional to the Rabi frequency (square root of the laser power) of the control field.

B. Coupling Model

We establish a model to describe the inter-channel coupling. We start from the full optical Bloch equations where the coherences and populations between any two atomic levels are included; then we adiabatically eliminate the excited-state dynamics. We further make the approximation that the populations of states $|1\rangle$ and $|2\rangle$ are 0 and 1, respectively, because the population of the excited state is nearly zero (since the control field's Rabi frequency is much smaller than the excited state's Doppler-broadened linewidth), and the control field is much stronger than the probe field.

As the optical coherence has a short lifetime of about 20 ns, we only consider the coupling between the ground-state coherences $\rho_{12}^{(1)}$ ($\rho_{12}^{(2)}$) for channel 1 (2). The coupling equation takes the form

$$\begin{cases} \dot{\rho}_{12}^{(1)} = -\gamma'_{12}\rho_{12}^{(1)} + \Gamma_c\rho_{12}^{(2)} - \frac{\Omega_c^{(1)*}\Omega_p^{(1)}}{\gamma_{23}}, \\ \dot{\rho}_{12}^{(2)} = -\gamma'_{12}\rho_{12}^{(2)} + \Gamma_c\rho_{12}^{(1)} - \frac{\Omega_c^{(2)*}\Omega_p^{(2)}}{\gamma_{23}}. \end{cases} \tag{4}$$

Here, $\gamma'_{12} = \gamma_{12} + \Gamma_c + \Gamma_p^{(1)} + \Gamma_p^{(2)}$ represents the total effective decay rate in each channel, with $\Gamma_p^{(i)} = \frac{|\Omega_c^{(i)}|^2}{\gamma_{23}}, i = 1, 2$ the optical pumping rate.

By setting $\dot{\rho}_{12}^{(1)} = \dot{\rho}_{12}^{(2)} = 0$, the steady-state solutions for the ground-state coherence are

$$\begin{cases} \rho_{12}^{(1)} = \frac{-\frac{\Omega_c^{(1)*}\Omega_p^{(1)}}{\gamma_{23}}\gamma'_{12} - \frac{\Omega_c^{(2)*}\Omega_p^{(2)}}{\gamma_{23}}\Gamma_c}{\gamma'^2_{12} - \Gamma_c^2}, \\ \rho_{12}^{(2)} = \frac{-\frac{\Omega_c^{(2)*}\Omega_p^{(2)}}{\gamma_{23}}\gamma'_{12} - \frac{\Omega_c^{(1)*}\Omega_p^{(1)}}{\gamma_{23}}\Gamma_c}{\gamma'^2_{12} - \Gamma_c^2}. \end{cases} \tag{5}$$

In an optical thin system, optical coherence $\rho_{32}^{(i)} = \frac{i\Omega_c^{(i)}\rho_{12}^{(i)} + i\Omega_p^{(i)}\rho_{22}^{(i)}}{\gamma_{23}}$, $\rho_{22}^{(i)} \approx 1, i = 1, 2$. According to the light propagating equation $\frac{dE^{(i)}}{dz} = \frac{i\bar{k}}{2}\chi^{(i)}E^{(i)} = \frac{N}{V}\frac{i\bar{k}}{2}\frac{\mu_0\rho_{32}^{(i)}}{\epsilon_0}$, we obtain the coupling equation of the probe fields

$$\begin{cases} \frac{dE^{(1)}}{dt} = \frac{Nc\bar{k}\mu_0^2}{2\hbar V\epsilon_0\gamma_{23}}\left(-E^{(1)}\gamma' + E^{(2)}\frac{\Gamma_c}{\gamma_{23}}\frac{\Omega_c^{(1)}\Omega_c^{(2)*}}{\gamma'^2_{12} - \Gamma_c^2}\right), \\ \frac{dE^{(2)}}{dt} = \frac{Nc\bar{k}\mu_0^2}{2\hbar V\epsilon_0\gamma_{23}}\left(-E^{(2)}\gamma' + E^{(1)}\frac{\Gamma_c}{\gamma_{23}}\frac{\Omega_c^{(2)}\Omega_c^{(1)*}}{\gamma'^2_{12} - \Gamma_c^2}\right), \end{cases} \tag{6}$$

where $\gamma' = 1 - \frac{|\Omega_c^{(i)}|^2\gamma'_{12}}{\gamma_{23}(\gamma'^2_{12} - \Gamma_c^2)}$, $\frac{N}{V}$ is the density of atoms, c is the speed of light in vacuum, $\bar{k}$ is the average wave vector, μ_0 is the dipole moment, and ϵ_0 is the vacuum dielectric constant. In the presence of the light wall, an atomic spin wave transported to the other channel induces an extra phase θ_0. Thus, Γ_c is replaced by $\Gamma_c e^{i\theta_0}$. Taking the coupling term into consideration, we have our beam-splitter Hamiltonian

$$\hat{H} = \hbar(g\hat{a}_1\hat{a}_2^\dagger - g^*\hat{a}_2^\dagger\hat{a}_1)e^{i\theta_0}, \tag{7}$$

where $g = -i\frac{Nc\bar{k}\mu_0^2\Gamma_c}{2\hbar V\epsilon_0\gamma_{23}^2}\frac{\Omega_c^{(2)*}\Omega_c^{(1)}}{\gamma'^2_{12} - \Gamma_c^2}$ is the complex coupling coefficient between the two probe fields. Here $\hat{a}_1$ ($\hat{a}_2$) is the annihilation operator for the probe field in Ch1 (Ch2).

To further understand the transport experiments, we assume $|\Omega_c^{(1)}| = |\Omega_c^{(2)}|$, and define $\gamma'' = \frac{Nc\bar{k}\mu_0^2}{2\hbar V\epsilon_0\gamma_{23}} \cdot \left(1 - \frac{|\Omega_c^{(i)}|^2\gamma'_{12}}{\gamma_{23}(\gamma'^2_{12} - \Gamma_c^2)}\right)$ and $\Gamma_c'' = \frac{Nc\bar{k}\mu_0^2}{2\hbar V\epsilon_0\gamma_{23}}\frac{\Gamma_c}{\gamma_{23}}\frac{\Omega_c^{(1)}\Omega_c^{(2)*}}{\gamma'^2_{12} - \Gamma_c^2}$. The coupling equations then become

$$\begin{cases} \frac{dE^{(1)}}{dt} = -\gamma''E^{(1)} + \Gamma_c''e^{i\theta_0}E^{(2)}, \\ \frac{dE^{(2)}}{dt} = -\gamma''E^{(2)} + \Gamma_c''^*e^{i\theta_0}E^{(1)}. \end{cases} \tag{8}$$

For the first scheme where only the probe field in Ch1 is switched on, we have (following a time-dependent perturbation)

$$\begin{cases} E_{p,\text{out}}^{(1)} = \left(1 - \frac{\gamma''L}{c}\right)E_{p,\text{in}}^{(1)}(t), \\ E_{p,\text{out}}^{(2)} = \frac{\Gamma_c''^*e^{i\theta_0}L}{c}E_{p,\text{in}}^{(1)}(t), \end{cases} \tag{9}$$

where L is the length of vapor cell. It follows that the detected intensities

$$\begin{cases} I_1(t) = \left|\left(1 - \frac{\gamma''L}{c}\right)E_{p,\text{in}}^{(1)}(t) + E_c^{(1)}\right|^2, \\ I_2(t) = \left|\frac{\Gamma_c''^*e^{i\theta_0}L}{c}E_{p,\text{in}}^{(1)}(t) + E_c^{(2)}\right|^2. \end{cases} \tag{10}$$

Since $\Gamma_c'' = |\Gamma_c''|e^{i(\phi_c^{(1)} - \phi_c^{(2)})}$, we have $I_1(t) \propto |1 + \beta_1 e^{i[\phi_p^{(1)}(t) - \phi_c^{(1)}]}|^2$ and $I_2(t) \propto |1 + \beta_2 e^{i[\phi_p^{(1)}(t) - \phi_c^{(1)} + \theta_0]}|^2$. Here constants $\beta_{1,2}$ are related to parameters of the system, and $\phi_{c,p}^1$ are the phases of the control and probe fields of Ch1.

For the second scheme where both probe fields are turned on, we only detect the probe fields in each channel's output,

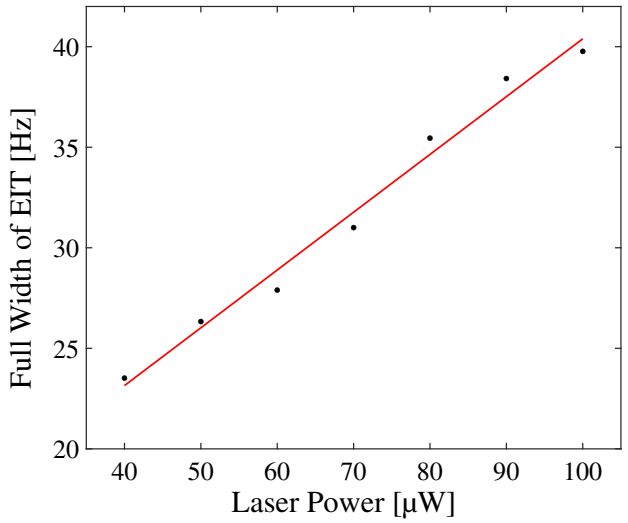

Fig. 6. Measured EIT linewidth versus laser power of the control field. The line is a linear fit to guide the eye.

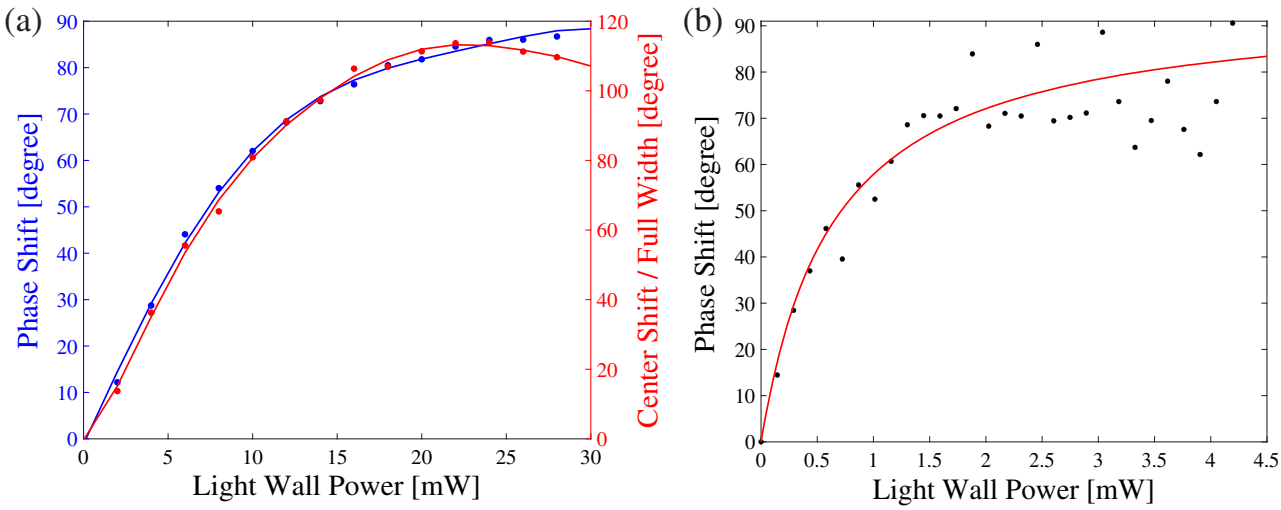

Fig. 7. (a) Experiment measurements of the phase saturation. Blue curve is the phase shift shown in Fig. 3(d). Red curve is the experimental EIT center shift divided by the EIT full linewidth. (b) Monte Carlo simulation results (black dots) of the phase shift. The red curve is a fit of the Monte Carlo results to guide the eye. The laser power required in the simulation is smaller than that in the experiment because the atomic motion in the model is two-dimensional and thus more phase shift accumulates for the same laser parameters.

with

$$\begin{cases} E_{p,\mathrm{out}}^{(1)} = \left(1-\frac{\gamma'' L}{c}\right) E_{p,\mathrm{in}}^{(1)}(t) + \frac{\Gamma_c'' e^{i\theta_0} L}{c} E_{p,\mathrm{in}}^{(2)}, \\ E_{p,\mathrm{out}}^{(2)} = \left(1-\frac{\gamma'' L}{c}\right) E_{p,\mathrm{in}}^{(2)}(t) + \frac{\Gamma_c''^{*} e^{i\theta_0} L}{c} E_{p,\mathrm{in}}^{(1)}(t). \end{cases} \tag{11}$$

The detected intensities are then

$$\begin{cases} I_1(t) \propto \left|1+\beta' e^{i[\phi_p^{(1)}(t)-\phi_c^{(1)}+\phi_c^{(2)}-\phi_p^{(2)}-\theta_0]}\right|^2, \\ I_2(t) \propto \left|1+\beta' e^{i[\phi_p^{(1)}(t)-\phi_c^{(1)}+\phi_c^{(2)}-\phi_p^{(2)}+\theta_0]}\right|^2. \end{cases} \tag{12}$$

Here the constant β' is related to parameters of the system, and $\phi_{c,p}^2$ are the phases of the control and probe fields of Ch2.

C. Phase Shift Saturation

As shown in Figs. 3(d) and 4(d), the phase shift caused by the light wall is not proportional to the light-wall power but saturates to a constant. However, the AC Stark shift caused by the far-detuned light is proportional to the light power, resulting in the linear relation between the EIT-center shift and the light-wall power in Fig. 2(c). To understand the relation between the phase shift and the light-wall power, we introduce an effective interaction time between the flying atoms and the light wall. The effective interaction time should correspond to the time it takes for the system to reach the steady state (denoted as t_{steady}), and should be approximately inversely proportional to the EIT full linewidth ω_{full}. Here the EIT linewidth $\omega_{\mathrm{full}} = \gamma_0 + \gamma_{p_l}$, where γ_0 is the EIT width without the light wall, and γ_{p_l} is the linewidth broadening due to the light wall (as shown in Fig. 1), proportional to the light wall's laser power. It follows that $t_{\mathrm{steady}} = \frac{1}{\gamma_0+\alpha_1 P}$. The phase picked up by the atomic spin wave corresponds to the EIT center shift $\alpha_2 P$ (which is also proportional to the light-wall power) times the effective interaction time. We then obtain $\theta_0 = \frac{\alpha_2 P}{\gamma_0+\alpha_1 P}$. When the light-wall power P is small, $\theta_0 \propto P$. As the power increases, θ_0 saturates to a constant.

In the experiment, we measure the EIT full linewidth and EIT center shift as functions of the light-wall power. The dependence of the phase shift on the light-wall power is similar to that of the EIT center shift divided by the EIT full linewidth, as shown in Fig. 7(a). To check these results theoretically, we carry out a two-dimensional Monte Carlo simulation. The model is similar to the one we developed in Ref. [48], but now we add a far-detuned laser region. The simulation results are shown in Fig. 7(b), which qualitatively agree with the experiment trends.

Funding. NSFC-ISF (12161141018); National Natural Science Foundation of China (11974331, 12027806, 61675047, 11874038); National Key Research and Development Program of China (2017YFA0304204, 2016YFA0301700, 2017YFA0304100, 2016YFA0302000).

Disclosures. The authors declare no conflicts of interest.

Data Availability. Data underlying the results presented in this paper are not publicly available at this time but may be obtained from the authors upon reasonable request.

REFERENCES

1. N. Moiseyev, *Non-Hermitian Quantum Mechanics* (Cambridge University, 2011).
2. Y. Ashida, Z. Gong, and M. Ueda, "Non-Hermitian physics," Adv. Phys. **69**, 249–435 (2020).
3. C. Bender and S. Boettcher, "Real spectra in non-Hermitian Hamiltonians having PT symmetry," Phys. Rev. Lett. **80**, 5243–5246 (1998).
4. R. El-Ganainy, K. Makris, M. Khajavikhan, Z. Musslimani, S. Rotter, and D. Christodoulides, "Non-Hermitian physics and PT symmetry," Nat. Phys. **14**, 11–19 (2018).
5. Ş. Özdemir, S. Rotter, F. Nori, and L. Yang, "Parity-time symmetry and exceptional points in photonics," Nat. Mater. **18**, 783–798 (2019).
6. M. Miri and A. Alú, "Exceptional points in optics and photonics," Science **363**, eaar7709 (2019).

7. H. Jing, Ş. Özdemir, Z. Geng, J. Zhang, X. Lü, B. Peng, L. Yang, and F. Nori, "Optomechanically-induced transparency in parity-time-symmetric microresonators," Sci. Rep. **5**, 9663 (2015).
8. F. Minganti, A. Miranowicz, R. Chhajlany, I. Arkhipov, and F. Nori, "Hybrid-Liouvillian formalism connecting exceptional points of non-Hermitian Hamiltonians and Liouvillians via postselection of quantum trajectories," Phys. Rev. A **101**, 062112 (2020).
9. I. Arkhipov, A. Miranowicz, F. Minganti, and F. Nori, "Liouvillian exceptional points of any order in dissipative linear bosonic systems: coherence functions and switching between PT and anti-PT symmetries," Phys. Rev. A **102**, 033715 (2020).
10. B. Peng, Ş. K. Özdemir, S. Rotter, H. Yilmaz, M. Liertzer, F. Monifi, C. Bender, F. Nori, and L. Yang, "Loss-induced suppression and revival of lasing," Science **346**, 328–332 (2014).
11. Z. Liu, J. Zhang, Ş. K. Özdemir, B. Peng, H. Jing, X. Lü, C. Li, L. Yang, F. Nori, and Y. Liu, "Metrology with PT-symmetric cavities: enhanced sensitivity near the PT-phase transition," Phys. Rev. Lett. **117**, 110802 (2016).
12. K. Kawabata, Y. Ashida, and M. Ueda, "Information retrieval and criticality in parity-time-symmetric systems," Phys. Rev. Lett. **119**, 190401 (2017).
13. B. Dóra, M. Heyl, and R. Moessner, "The Kibble-Zurek mechanism at exceptional points," Nat. Commun. **10**, 2254 (2019).
14. B. Zhou, R. Wang, and B. Wang, "Renormalization group approach to non-Hermitian topological quantum criticality," Phys. Rev. B **102**, 205116 (2020).
15. X. Bao, G. Guo, X. Du, H. Gu, and L. Tan, "The topological criticality in disordered non-Hermitian system," J. Phys. Condens. Matter **33**, 185401 (2021).
16. S. Yao and Z. Wang, "Edge states and topological invariants of non-Hermitian systems," Phys. Rev. Lett. **121**, 086803 (2018).
17. F. Kunst, E. Edvardsson, J. Budich, and E. Bergholtz, "Biorthogonal bulk-boundary correspondence in non-Hermitian systems," Phys. Rev. Lett. **121**, 026808 (2018).
18. V. Alvarez, J. Barrios, and L. Torres, "Non-Hermitian robust edge states in one dimension: anomalous localization and eigenspace condensation at exceptional points," Phys. Rev. B **97**, 121401 (2018).
19. A. McDonald, T. Pereg-Barnea, and A. Clerk, "Phase-dependent chiral transport and effective non-Hermitian dynamics in a bosonic Kitaev-Majorana chain," Phys. Rev. X **8**, 041031 (2018).
20. C. Lee and R. Thomale, "Anatomy of skin modes and topology in non-Hermitian systems," Phys. Rev. B **99**, 201103 (2019).
21. T. Lee, "Anomalous edge state in a non-Hermitian lattice," Phys. Rev. Lett. **116**, 133903 (2016).
22. S. Yao, F. Song, and Z. Wang, "Non-Hermitian Chern bands," Phys. Rev. Lett. **121**, 136802 (2018).
23. K. Yokomizo and S. Murakami, "Non-Bloch band theory of non-Hermitian systems," Phys. Rev. Lett. **123**, 066404 (2019).
24. L. Li, C. Lee, S. Mu, and J. Gong, "Critical non-Hermitian skin effect," Nat. Commun. **11**, 5491 (2020).
25. Z. Gong, Y. Ashida, K. Kawabata, K. Takasan, S. Higashikawa, and M. Ueda, "Topological phases of non-Hermitian systems," Phys. Rev. X **8**, 031079 (2018).
26. D. Leykam, K. Bliokh, C. Huang, Y. Chong, and F. Nori, "Edge modes, degeneracies, and topological numbers in non-Hermitian systems," Phys. Rev. Lett. **118**, 040401 (2017).
27. T. Liu, Y. Zhang, Q. Ai, Z. Gong, K. Kawabata, M. Ueda, and F. Nori, "Second-order topological phases in non-Hermitian systems," Phys. Rev. Lett. **122**, 076801 (2019).
28. T. Liu, J. He, T. Yoshida, Z. Xiang, and F. Nori, "Non-Hermitian topological Mott insulators in one-dimensional fermionic superlattices," Phys. Rev. B **102**, 235151 (2020).
29. W. Nie, M. Antezza, Y. Liu, and F. Nori, "Dissipative topological phase transition with strong system-environment coupling," Phys. Rev. Lett. **127**, 250402 (2021).
30. L. Xiao, X. Zhan, H. Bian, K. Wang, X. Zhang, P. Wang, J. Li, K. Mochizuki, D. Kim, N. Kawakami, W. Yi, H. Obuse, C. Sanders, and P. Xue, "Observation of topological edge states in parity-time-symmetric quantum walks," Nat. Phys. **13**, 1117–1123 (2017).
31. L. Xiao, K. Wang, X. Zhan, Z. Bian, K. Kawabata, M. Ueda, W. Yi, and P. Xue, "Observation of critical phenomena in parity-time-symmetric quantum dynamics," Phys. Rev. Lett. **123**, 230401 (2019).
32. L. Xiao, T. Deng, K. Wang, G. Zhu, Z. Wang, W. Yi, and P. Xue, "Non-Hermitian bulk-boundary correspondence in quantum dynamics," Nat. Phys. **16**, 761–766 (2020).
33. K. Zhao, M. Schaden, and Z. Wu, "Enhanced magnetic resonance signal of spin-polarized Rb atoms near surfaces of coated cells," Phys. Rev. A **81**, 042903 (2010).
34. Z. Zhang, Y. Zhang, J. Sheng, L. Yang, M. Mili, D. Christodoulides, B. He, Y. Zhang, and M. Xiao, "Observation of parity-time symmetry in optically induced atomic lattices," Phys. Rev. Lett. **117**, 123601 (2016).
35. J. Li, A. Harter, J. Liu, L. de Melo, Y. N. Joglekar, and L. Luo, "Observation of parity-time symmetry breaking transitions in a dissipative Floquet system of ultracold atoms," Nat. Commun. **10**, 855 (2019).
36. S. Lapp, J. Angonga, F. A. An, and B. Gadway, "Engineering tunable local loss in a synthetic lattice of momentum states," New J. Phys. **21**, 045006 (2019).
37. W. Gou, T. Chen, D. Xie, T. Xiao, T. Deng, B. Gadway, W. Yi, and B. Yan, "Tunable nonreciprocal quantum transport through a dissipative Aharonov-Bohm ring in ultracold atoms," Phys. Rev. Lett. **124**, 070402 (2020).
38. T. Chen, W. Gou, D. Xie, T. Xiao, W. Yi, J. Jing, and B. Yan, "Quantum Zeno effects across a parity-time symmetry breaking transition in atomic momentum space," npj Quantum Inf. **7**, 78 (2021).
39. Z. Ren, D. Liu, E. Zhao, C. He, K. K. Pak, J. Li, and G. Jo, "Topological control of quantum states in non-Hermitian spin-orbit-coupled fermions," Nat. Phys. **18**, 385–389 (2022).
40. P. Peng, W. Cao, C. Shen, W. Qu, J. Wen, L. Jiang, and Y. Xiao, "Anti-parity-time symmetry with flying atoms," Nat. Phys. **12**, 1139–1145 (2016).
41. T. Gao, E. Estrecho, K. Bliokh, T. Liew, M. Fraser, S. Brodbeck, M. Kamp, C. Schneider, S. Höfling, and Y. Yamamoto, "Observation of non-Hermitian degeneracies in a chaotic exciton-polariton billiard," Nature **526**, 554–558 (2015).
42. Y. Wu, W. Liu, J. Geng, X. Song, X. Ye, C. Duan, X. Rong, and J. Du, "Observation of parity-time symmetry breaking in a single-spin system," Science **364**, 878–880 (2019).
43. W. Liu, Y. Wu, C. Duan, X. Rong, and J. Du, "Dynamically encircling an exceptional point in a real quantum system," Phys. Rev. Lett. **126**, 170506 (2021).
44. W. Wang, Y. Zhou, H. Zhang, J. Zhang, M. Zhang, Y. Xie, C. Wu, T. Chen, B. Ou, W. Wu, H. Jing, and P. Chen, "Observation of PT-symmetric quantum coherence in a single-ion system," Phys. Rev. A **103**, L020201 (2021).
45. L. Ding, K. Shi, Q. Zhang, D. Shen, X. Zhang, and W. Zhang, "Experimental determination of PT-symmetric exceptional points in a single trapped ion," Phys. Rev. Lett. **126**, 083604 (2021).
46. M. Naghiloo, M. Abbasi, Y. N. Jogelkar, and K. W. Murch, "Quantum state tomography across the exceptional point in a single dissipative qubit," Nat. Phys. **15**, 1232–1236 (2019).
47. M. Lukin, "Colloquium: trapping and manipulating photon states in atomic ensembles," Rev. Mod. Phys. **75**, 457–472 (2003).
48. W. Cao, X. Lu, X. Meng, J. Sun, H. Shen, and Y. Xiao, "Reservoir-mediated quantum correlations in non-Hermitian optical system," Phys. Rev. Lett. **124**, 030401 (2020).
49. X. Lu, W. Cao, W. Yi, H. Shen, and Y. Xiao, "Nonreciprocity and quantum correlations of light transport in hot atoms via reservoir engineering," Phys. Rev. Lett. **126**, 223603 (2021).
50. Y. Xiao, M. Klein, M. Hohensee, L. Jiang, D. Philips, M. Lukin, and R. Walsworth, "Slow light beam splitter," Phys. Rev. Lett. **101**, 043601 (2008).
51. R. Campos, B. Saleh, and M. Teich, "Quantum-mechanical lossless beam splitter: SU(2) symmetry and photon statistics," Phys. Rev. A **40**, 1371–1384 (1989).
52. S. M. Barnett, J. Jekers, and A. Gatti, "Quantum optics of lossy beam splitters," Phys. Rev. A **57**, 2134–2145 (1998).

53. M. Balabas, T. Karaulanov, M. Ledbetter, and D. Budker, "Polarized alkali-metal vapor with minute-long transverse spin-relaxation time," Phys. Rev. Lett. **105**, 070801 (2010).
54. O. Firstenberg, M. Shuker, A. Ron, and N. Davidson, "Coherent diffusion of polaritons in atomic media," Rev. Mod. Phys. **85**, 941–960 (2013).
55. J. Borregaard, M. Zugenmaier, J. Petersen, H. Shen, G. Vasilakis, K. Jensen, E. Polzik, and A. Sørensen, "Scalable photonic network architecture based on motional averaging in room temperature gas," Nat. Commun. **7**, 11356 (2016).
56. T. Abi-Salloum, "Electromagnetically induced transparency and Autler-Townes splitting: two similar but distinct phenomena in two categories of three-level atomic systems," Phys. Rev. A **81**, 053836 (2010).
57. H. Sun, Y. Liu, H. Ian, J. You, E. Il'ichev, and F. Nori, "Electromagnetically inducd transparency and Autler-Townes splitting in superconducting flux quantum circuits," Phys. Rev. A **89**, 063822 (2014).
58. B. Peng, Ş. K. Özdemir, W. Chen, F. Nori, and L. Yang, "What is and what is not electromagnetically induced transparency in whispering-gallery microcavities," Nat. Commun. **5**, 5082 (2014).
59. Q. Liu, T. Li, X. Luo, H. Zhao, W. Xiong, Y. Zhang, Z. Chen, J. Liu, W. Chen, and F. Nori, "Method for identifying electromagnetically induced transparency in a tunable circuit quantum electrodynamics system," Phys. Rev. A **93**, 053838 (2016).
60. L. He, Y. Liu, S. Yi, C. Sun, and F. Nori, "Control of photon propagation via electromagnetically induced transparency in lossless media," Phys. Rev. A **75**, 063818 (2007).
61. R. Wen, C. Zou, X. Zhu, P. Chen, Z. Ou, J. Chen, and W. Zhang, "Non-Hermitian magnon-photon interference in an atomic ensemble," Phys. Rev. Lett. **122**, 253602 (2019).
62. X. Huang, C. Lu, C. Liang, H. Tao, and Y. Liu, "Loss-induced nonreciprocity," Light Sci. Appl. **10**, 30 (2021).
63. D. Hao, L. Wang, X. Lu, X. Cao, S. Jia, Y. Hu, and Y. Xiao, "Topological atomic spinwave lattices by dissipative couplings," arXiv:2203.15288 (2022).
64. D. Jalas, A. Petrov, M. Eich, W. Freude, S. Fan, Z. Yu, R. Baets, M. Popovic, A. Melloni, J. Joannopoulos, M. Vanwolleghem, C. Doerr, and H. Renner, "What is—and what is not—an optical isolator," Nat. Photonics **7**, 579–582 (2013).
65. L. Tzuang, K. Fang, P. Nussenzveig, S. Fan, and M. Lipson, "Non-reciprocal phase shift induced by an effective magnetic flux for light," Nat. Photonics **8**, 701–705 (2014).
66. A. Metelmann and A. Clerk, "Nonreciprocal photon transmission and amplification via reservoir engineering," Phys. Rev. X **5**, 021025 (2015).
67. L. Bao, B. Qi, D. Dong, and F. Nori, "Fundamental limits for reciprocal and nonreciprocal non-Hermitian quantum sensing," Phys. Rev. A **103**, 042418 (2021).
68. L. Tang, J. Tang, M. Chen, F. Nori, M. Xiao, and K. Xia, "Quantum squeezing induced optical nonreciprocity," Phys. Rev. Lett. **128**, 083604 (2022).
69. G. Arwas, S. Gadasi, I. Gershenzon, A. Friesem, N. Davidson, and O. Raz, "Anyonic parity-time symmetric laser," Sci. Adv. **8**, 7454 (2022).
70. K. Kim, M. Sujak, E. Kang, and Y. No, "Tunable non-Hermiticity in coupled photonic crystal cavities with asymmetric optical gain," Appl. Sci. **10**, 8074 (2020).
71. J. Sun, X. Zhang, W. Qu, E. Mikhailov, I. Novikova, H. Shen, and Y. Xiao, "Spatial multiplexing of squeezed light by coherence diffusion," Phys. Rev. Lett. **123**, 203604 (2019).